Reversible Spin-State Switching and Tuning of Nuclearity and Dimensionality via Nonlinear Pseudohalides in Cobalt(II) Complexes

Subrata Ghosh, Sujit Kamilya, Mathieu Rouzières, Radovan Herchel, Sakshi Mehta, Abhishake Mondal

Reversible Spin-State Switching and Tuning of Nuclearity and Dimensionality via Nonlinear Pseudohalides in Cobalt(II) Complexes

Subrata Ghosh, Sujit Kamilya, Mathieu Rouzières, Radovan Herchel, Sakshi Mehta, and Abhishake Mondal*

ABSTRACT: The self-assembly of a macrocyclic tetradentate ligand, cobalt(II) tetrafluoroborate, and nonlinear pseudohalides (dicyanamide and tricyanomethanide) has led to two cobalt(II) complexes, $\{[Co(\mathbf{L})(\mu_{1,5}\text{-dca})](BF_4)\cdot MeOH\}_n$ (**1**) and $[Co_2(\mathbf{L})_2(\mu_{1,5}\text{-tcm})_2](BF_4)_2$ (**2**) (**L** = *N*,*N*′-di-*tert*-butyl-2,11-diaza[3,3](2,6)pyridinophane; dca^- = dicyanamido; tcm^- = tricyanomethanido). Both complexes were characterized by single-crystal X-ray diffraction, spectroscopic, magnetic, and electrochemical studies. Structural analyses revealed that **1** displays a one-dimensional (1D) coordination polymer containing $[Co(\mathbf{L})]^{2+}$ repeating units bridged by $\mu_{1,5}$-dicyanamido groups in *cis* positions, while **2** represents a discreate dinuclear cobalt(II) molecule bridged by two $\mu_{1,5}$-tricyanomethanido groups in a *cis* conformation. Both complexes have a CoN_6 coordination environment around each cobalt center offered by the tetradentate ligand and *cis* coordinating bridging ligands. Complex **1** exhibits a high-spin (S = 3/2) state of cobalt(II) in the temperature range of 2−300 K with a weak ferromagnetic coupling between two dicyanamido-bridged cobalt(II) centers. Interestingly, complex **2** exhibits reversible spin-state switching associated with spin−spin coupling. Complexes **1** and **2** also exhibit interesting redox-stimuli-based reversible paramagnetic high-spin cobalt(II) to diamagnetic low-spin cobalt(III) conversion, offering an additional way to switch magnetic properties. A detailed theoretical calculation was consistent with the stated results.

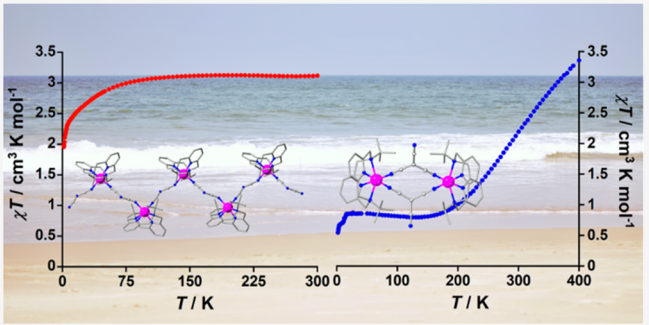

INTRODUCTION

Low-dimensional multifunctional magnetic systems possess unique advantages of having chemical control over numerous physical properties. These attributes lead to amazing applications to storing and processing quantum information.[1,2] All of these fascinating systems are of great interest in the material sciences for their potential applications in switches and sensors, as the physical properties of such systems can be controlled and tuned by the application of various external stimuli.[3−7] Among those, switchable bistable materials based on transition metals have attained an enormous importance over the last few decades, particularly materials displaying magnetic or electric bistabilities such as spin crossover (SCO),[8−11] single-molecule magnets (SMMs),[12−17] single chain magnets (SCMs),[18−20] metal-to-metal electron transfer,[21−26] organic radicals,[27,28] etc. SCO materials represent emerging candidates over the past few decades offering an attractive route to the realization of molecular spintronics, molecular sensors, and nanoscale devices.[29−33] It is well-known for the SCO systems that the electronic conversion between two easily accessible low-spin (LS) and high-spin (HS) states can be tuned or manipulated in a reversible manner under a slight modification of external perturbation: e.g. temperature, pressure, light irradiation, magnetic field, etc.[34−38] The SCO systems exhibit spectacular differences in their magnetic, conductive, optical, and other physicochemical properties.

To date, complexes based on iron(II) and iron(III) represent the most studied SCO systems;[39−48] in contrast, SCO systems based on d^7 cobalt(II) are less common.[49−53] Above all, the interesting light-induced excited spin state trapping (LIESST) effect has not been observed so far in cobalt(II) SCO systems. For cobalt(II) in an octahedral geometry, spin-state switching occurs between the LS ($t^6_{2g}e^1_g$, S = 1/2, ^2E) and the HS ($t^5_{2g}e^2_g$, S = 3/2, $^4T_1$) states. The magnitude and direction of structural changes that are associated with SCO in cobalt(II) vary significantly from those observed in iron(II) due to an uneven distribution of electrons in the e_g orbitals of the LS state of cobalt(II) that is greatly affected by Jahn−Teller distortion in an octahedral geometry.[54] In addition, cobalt(II) induces a faster

Scheme 1. Schematic Presentation of Macrocyclic Ligand L and Synthetic Route of 1 and 2

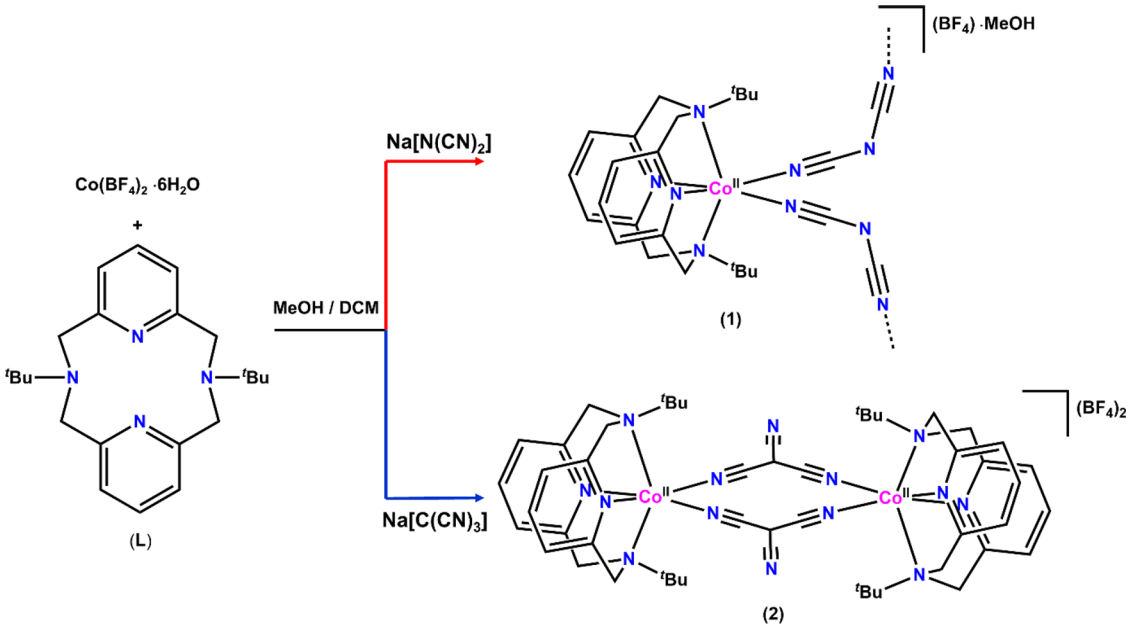

spin transition dynamics and high sensitivity toward the lattice environment, counteranion, and crystalline solvent molecules. This is due to the presence of a small energy gap between the potential energy surfaces of the HS and LS states. These characteristics of the cobalt(II) system offer both challenges and opportunities to design and synthesize novel cobalt(II) SCO complexes. Indeed, ligands with an appropriate ligand-field strength for spin-state switching in cobalt(II) center are rare. However, a ligand based on terpyridine and its derivatives have been used intensively.[51,55−57] It is reported that the coordination environment around a cobalt(II) center having a CoN_6 surrounding with all six donating nitrogen atoms coming from two neutral tridentate ligands generates $[Co(L\text{-}N_3)_2]^{2+}$ SCO complexes. In addition, extremely rare reports have explored the SCO properties of cobalt(II) with ligand systems different from terpyridine.[58−62]

The potential of linear or nonlinear pseudohalides to tune the ligand field strength in SCO cobalt(II) systems has been rarely explored[61−64] but has been relatively well studied in various areas of SCO iron systems.[41,65,66] It is worth mentioning that we have currently reported mononuclear cobalt(II) SCO complexes based on a tetradentate macrocyclic neutral ligand that provides four nitrogen atoms with two other nitrogen atoms coming from linear or nonlinear pseudohalides (NCX^-) to produce a CoN_6 coordination environment of the SCO cobalt(II) center.[63,64] The use of nonlinear pseudohalide should allow us to explore a magnetostructural diversity, since the molecular structure of a complex with the desired nuclearity and/or dimension can be rationally designed using various judiciously chosen nonlinear pseudohalides as bridging ligands.[67] Additionally, this process should allow us to explore another interesting aspect, the coexistence of SCO and intramolecular spin exchange interactions in a single molecular system. This has not yet been developed in a cobalt system. So far, dinuclear SCO complexes represent simple systems having both exciting properties operational in a synergic fashion. To the best of our knowledge, only two dinuclear cobalt(II) SCO complexes based on neutral bridging ligands have been reported to date, which show an incomplete SCO behavior at high temperature (only ∼25% conversion).[68,69]

In this work we are interested in exploring and correlating the effect of pseudohalides (dicyanamido and tricyanomethanido) as bridging ligands in association with a neutral tetradentate macrocyclic chelating ligand. This will lead to a significant modification of molecular dimensions, nuclearity, and physical properties of the resulting cobalt(II) complexes. Herein, we report the syntheses, variable-temperature crystal structures, magnetic, spectroscopic, and electrochemical properties, and detailed theoretical investigations of the two new cobalt(II) complexes $\{[Co(\mathbf{L})(\mu_{1,5}\text{-dca})](BF_4)\cdot MeOH\}_n$ (**1**) and $[Co_2(\mathbf{L})_2(\mu_{1,5}\text{-tcm})_2](BF_4)_2$ (**2**) (**L** = *N*,*N*′-di-*tert*-butyl-2,11-diaza[3,3](2,6)pyridinophane; dca^- = dicyanamido; tcm^- = tricyanomethanido).

RESULTS AND DISCUSSION

Synthesis and Characterization. The reaction of a mixture of $Co(BF_4)_2\cdot 6H_2O$ and macrocyclic ligand **L** with 1 equiv of $Na[N(CN)_2]$ and $Na[C(CN)_3]$ in a mixture of methanol and dichloromethane afforded a pink and an orange solution, respectively. After filtration, slow evaporation of the filtrate yielded **1** and **2** as pink and orange crystals in good yield (Scheme 1 and Figure 1). Elemental analyses and PXRD studies have been performed to confirm the purity of both the complexes (Figures S1 and S2). Thermogravimetry analysis plots (Figure S3) show that complex **1** undergoes a weight loss

Figure 1. Images of crystals of complexes **1** (left) and **2** (right).

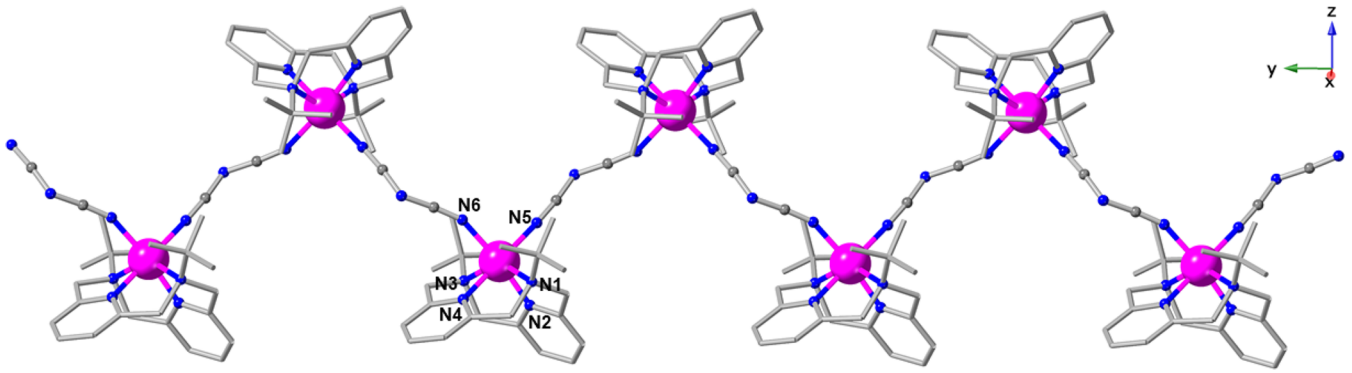

Figure 2. Perspective view of the 1D coordination polymer in **1** at 296 K. Counteranions, solvent molecules, and hydrogen atoms are omitted for clarity (Co, pink; C, gray; N, blue).

between 450 and 470 K (ca. 5.5%) corresponding to the release of one methanol molecule as an interstitial solvent, while complex **2** exhibits a thermal stability up to around 470 K, indicating the absence of a crystallized solvent molecule. These results were further confirmed by single-crystal structure analyses (*vide infra*).

Complexes **1** and **2** were well characterized by solid-state IR spectroscopy at room temperature (Figures S4 and S5). For complexes containing pseudohalides as coligands with metal-coordinated N≡C bonds, IR spectroscopy serves as an important tool to characterize the oxidation state and the spin state of the metal center, as the cyanide stretching frequency ($\nu_{N\equiv C}$) is significantly altered by the electronic and spin states of the coordinated metal center. In addition, the positions of N≡C stretching frequencies can identify the different bonding modes for $[N(CN)_2]^-$ and $[C(CN)_3]^-$ coligands. Cobalt(II) complexes containing $[N(CN)_2]^-$ and $[C(CN)_3]^-$ as coligands or bridging ligands have been relatively less explored. The spectrum of $Na[N(CN)_2]$ displays three strong bands at 2285, 2228, and 2178 cm^{-1} for $\nu_{as}+\nu_s$(C−N), ν_{as}(C≡N) and ν_s(C≡N), respectively (Figure S5). Monodentate coordination of $[N(CN)_2]^-$ through a cyanide N atom shows two ν(C≡N) bands in the range 2160−2175 cm^{-1} (ν_s(C≡N)) and 2220−2235 cm^{-1} (ν_{as}(C≡N)), and the $\mu_{1,5}$-bidentate coordination mode shows these cyanide stretching vibrations at higher values.[70] In our previous report,[63] we showed that the mononuclear complex $[Co(\mathbf{L})(N(CN)_2)_2]$ is in a HS state at room temperature and shows two split peaks at 2158, 2166 cm^{-1} and 2219, 2222 cm^{-1} and a sharp peak at 2268 cm^{-1}. The IR spectrum of **1** displays intense peaks at around 2313, 2243, 2190, and 2171 cm^{-1} suggesting a *cis* $\mu_{1,5}$-bidentate coordination of $[N(CN)_2]^-$ with the HS state of the cobalt(II) center.

Similarly, tricyanomethanide monodentate coordination of $[C(CN)_3]^-$ through a cyanide N atom displays three ν(C≡N) bands at around 2230, 2200, and 2175 cm^{-1}, and $\mu_{1,5}$-bidentate coordination mode exhibits these vibrations at higher values in the ranges of 2250−2240 and 2205−2185 cm^{-1},[70] whereas the spectrum of $Na[C(CN)_3]$ shows three strong bands at around 2240, 2198, and 2168 cm^{-1} (Figure S5). The IR spectrum of **2** exhibits a sharp peak at 2193 cm^{-1} with two shoulders at around 2224 and 2171 cm^{-1} which suggests a *cis* $\mu_{1,5}$-bidentate coordination of $[C(CN)_3]^-$ and is a clear indication of the absence of a LS state here. In addition, complexes **1** and **2** are both cationic in nature, having BF_4^- as counteranions. The stretching vibrations of BF_4^- are found at around 1094, 1060, and 1027 cm^{-1}. The sharp peak at around 3523 cm^{-1} is ascribed to the ν(O−H) vibration from the crystallized methanol molecule in **1**. Moreover, both complexes display characteristic absorptions at around 1600, 1470, 1440, 1377, 1253, 1190, 1075, 851, and 760 cm^{-1} coming from the coordinated ligand **L** which are shifted to a higher energy in comparison to the free ligand, thereby confirming the coordination to the metal centers.

Crystal Structure Analyses. X-ray diffraction analyses were performed on suitable single crystals at 296 K (**1** and **2**) and 100 K (**2**) (Tables S1 and S2). Complex **1** crystallizes in the orthorhombic space group *Pbca*, while the orthorhombic space group *Pnma* is found in **2**. The crystal structure of **1** consists of $[Co(\mathbf{L})]^{2+}$ units bridged by $\mu_{1,5}$-dicyanamido groups in *cis* positions to form a 1D coordination polymer extended along the *a* axis and one BF_4^- ion together with one methanol molecule (Figures 2 and 3 and Figure S6). The crystal structure of **2**

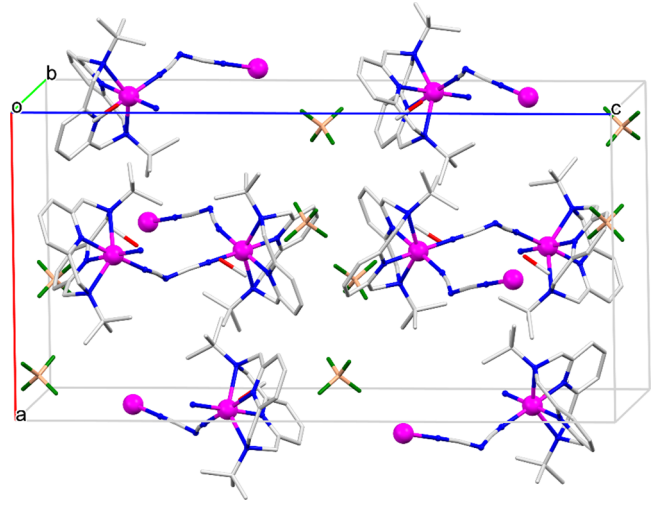

Figure 3. Unit cell packing diagram of **1** at 296 K. Hydrogen atoms are omitted for clarity (Co, pink; C, gray, N, blue; B, light pink; F, green; O, red).

contains the dinuclear dicationic species $[Co_2(\mathbf{L})_2(\mu_{1,5}\text{-tcm})_2]^{2+}$ and two BF_4^- anions per formula unit. Both cobalt centers are coordinated with the ligand **L** and bridged by two $[C(CN)_3]^-$ pseudohalides which act as $\mu_{1,5}$-bridging ligands via two cyanide groups (Figures 4 and 5 and Figure S6). No solvent molecule is detected in the crystal lattice, which is consistent with the TGA data (*vide supra*).

In both complexes, the amine and pyridine nitrogen donor atoms occupy the axial and equatorial positions, respectively, while the remaining equatorial positions are occupied by the

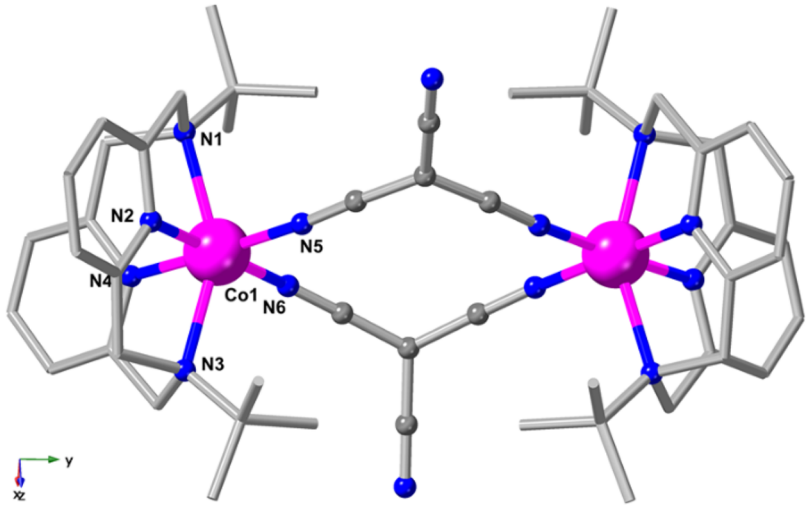

Figure 4. Perspective view of the complex cation in **2** at 296 K. Counteranions and hydrogen atoms are omitted for clarity (Co, pink; C, gray; N, blue).

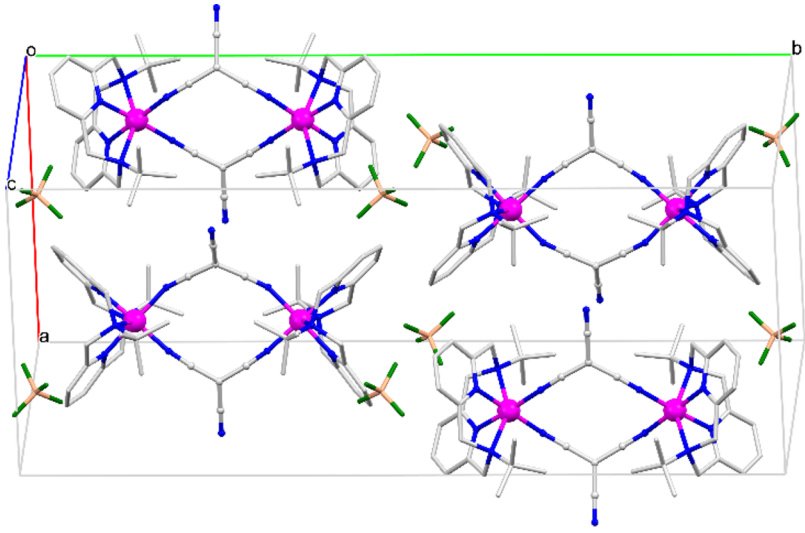

Figure 5. Unit cell packing diagram of **2** at 296 K. Hydrogen atoms are omitted for clarity (Co, pink; C, gray; N, blue; B, light pink; F, green).

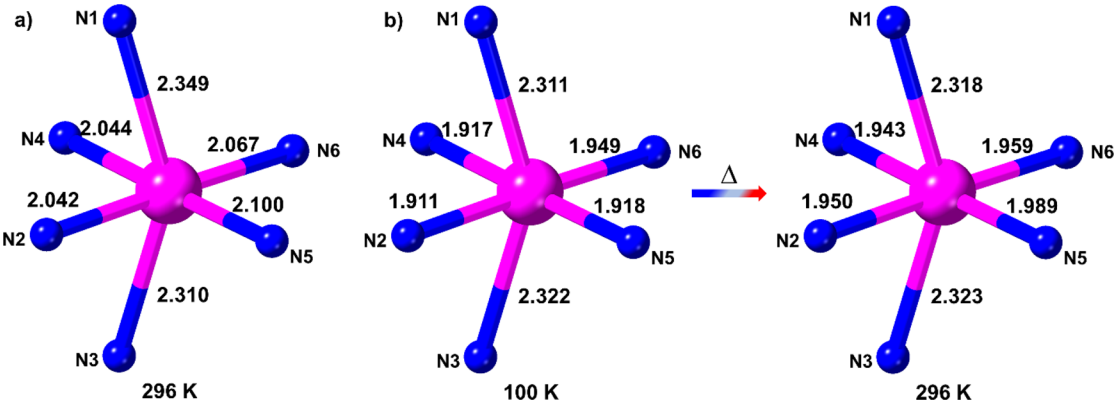

Figure 6. Comparison of Co−N distances in **1** at 296 K (a) and **2** at 100 and 296 K (b).

bridging pseudohalides. The cobalt centers lie in distorted-octahedral CoN_6 environments (continuous shape measures (CShM) program[71] (Table S3)), where the cobalt centers are coordinated to the four nitrogen donor atoms of the macrocyclic ligand **L** and two nitrogen donor atoms of two bridging ligands.

In complex **1** at 296 K, the axial Co−N_{am} bonds are significantly longer than the equatorial Co−N_{Py} and Co−N_{dca} bonds with average distances of 2.329, 2.043, and 2.083 Å, respectively (Figure 6, Table 1, and Table S2). The Co−N bond distances are very similar to those obtained in octahedral HS cobalt(II) complexes.[53,63,64,72,73] The N_{am}−Co−N_{am} angle

Table 1. Selected Bond Lengths, Bond Angles, and Structural Parameters for 1 and 2

	1	2	
T/K	296	296	100
Co−N_{am}/Å	2.349(3), 2.310(3)	2.318(2), 2.323(3)	2.311(2), 2.322(2)
Co−N_{Py}/Å	2.042(3), 2.044(2)	1.950(2), 1.943(3)	1.911(2), 1.917(2)
Co−N_{NCX}/Å	2.100(3), 2.067(3)	1.989(3), 1.959(3)	1.918(2), 1.949(2)
⟨Co−N⟩/Å	2.152	2.080	2.054
cis ∠N−Co−N/deg	75.2(1)−107.7(1)	77.5(1)−104.3(1)	78.38(6)−104.03(7)
trans ∠N−Co−N/deg	144.15(9)−178.9(1)	149.25(9)−177.6(1)	151.09(6)−177.81(7)
Co−N−C(X)/deg	156.0(3), 156.0(3)	157.6(3), 169.7(3)	157.2(2), 170.7(2)
N−C−X_{NCX}/deg	173.7(4), 173.7(4)	177.0, 175.4	175.0, 177.1
∑Co/deg	111.21	93.4	88.66
θ_{Co}/deg	338.48	306.31	296.41
ζ/Å	0.707	0.961	1.046
CShM (O_h)	2.428	2.365	2.277

significantly deviates from linearity (180°) to 144.15(9)°, while N_{Py}−Co−N_{Py} and N_{dca}−Co−N_{dca} angles in the equatorial plane are slightly deviated from 90° to 87.3(1) and 92.7(1)°, respectively (Table 1 and Table S2). The bridging arrangement Co−NC−N−CN−Co acquires a V-shaped conformation with a C(1)−N(7)−C(2) angle having a value of 125.3(3)°, while N−C−N angles are almost linear with values of 173.1(3) and 171.7(3)° (for N(5)−C(1)−N(7) and N(6)−C(2)−N(7), respectively). In addition, the Co−N(5)−C(1) angle of 156.3(2)° deviates from linearity while the Co−N(6)−C(2) angle is nearly linear with a value of 177.2(2)°. The Co···Co distance between two $\mu_{1,5}$-dicyanamide-bridged cobalt centers is 8.379 Å.

The average Co−N bond distance in **2** at 296 K is 2.080 Å with typical bond distance values of 2.320, 1.946, and 1.974 Å for Co−N_{am}, Co−N_{Py}, and Co−N_{tcm}, respectively (Figure 6, Table 1, and Table S2). This value is significantly lower than that observed in **1** (2.151 Å) but larger than that expected for an octahedral LS cobalt(II) system.[53,58,63,64] This illustrates that the cobalt(II) center in complex **2** is not completely in an LS state; rather, it is in a mixture of cobalt(II) HS/LS states at 296 K. When the temperature is decreased to 100 K, the overall structural motif of **2** remains nearly identical (Figure S6); however, a spectacular difference occurs in the cobalt(II) coordination surroundings. The most noticeable change is the decrease in Co−N bond distances (Figure 6). At 100 K, the average value of the Co−N bond distance decreases slightly to 2.054 Å (Δ = 0.036 Å) with average Co−N_{am}, Co−N_{Py}, and Co−N_{tcm} bond distances of 2.316, 1.914, and 1.933 Å, respectively (Figure 6, Table 1, and Table S2). These values fall in the range of that expected for cobalt(II) LS complexes.[53,58,63,64] Similar to our previous report on cobalt(II) SCO complexes with the tetradentate macrocyclic ligand **L**,[63,64] a significant change was noticed only in the equatorial Co−N bonds, while the axial Co−N bonds remain almost unchanged. This can be explained by tetrahedral distortion and Jahn−Teller effects present in the complex. These facts can be described by the following: for a cobalt(II) complex in an octahedral system, the d_{z^2} and $d_{x^2-y^2}$ orbitals are singly occupied in the HS state while a depopulation of the $d_{x^2-y^2}$ orbital takes place during the HS to LS spin-crossover process. As a result, a significant shortening of the bond distances in the *xz* plane has been observed in the LS state in comparison to the HS state. In contrast, the d_{z^2} orbital remains in a singly populated state regardless of the spin state. Thus, the bond distances along the *z* direction is unaffected or slightly affected. Indeed, equatorial

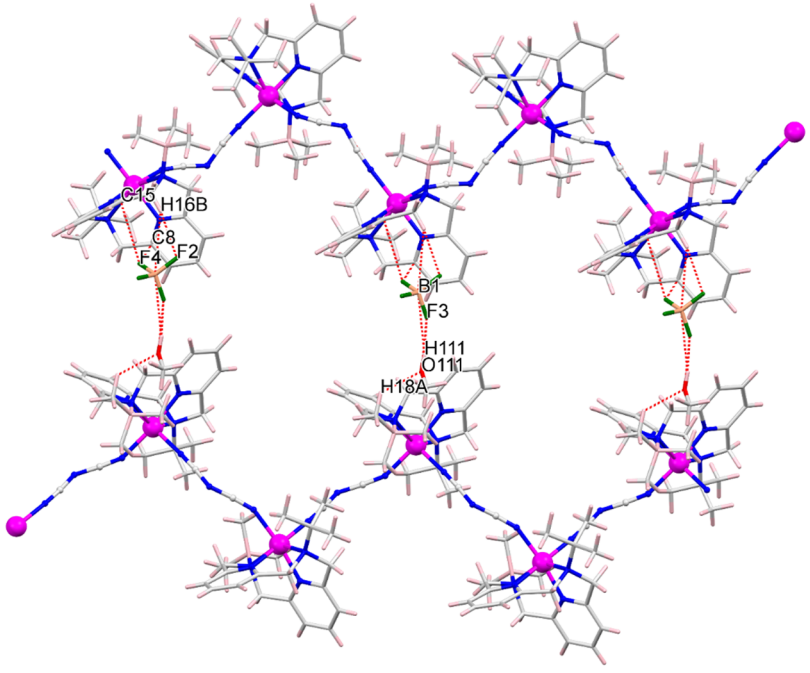

Figure 7. Packing diagram of **1** at 296 K showing the supramolecular double chain (bottom) formed by several C−H···F and C·····F (red dotted lines) interactions (Co, pink; C, gray; N, blue; B, light pink; F, green).

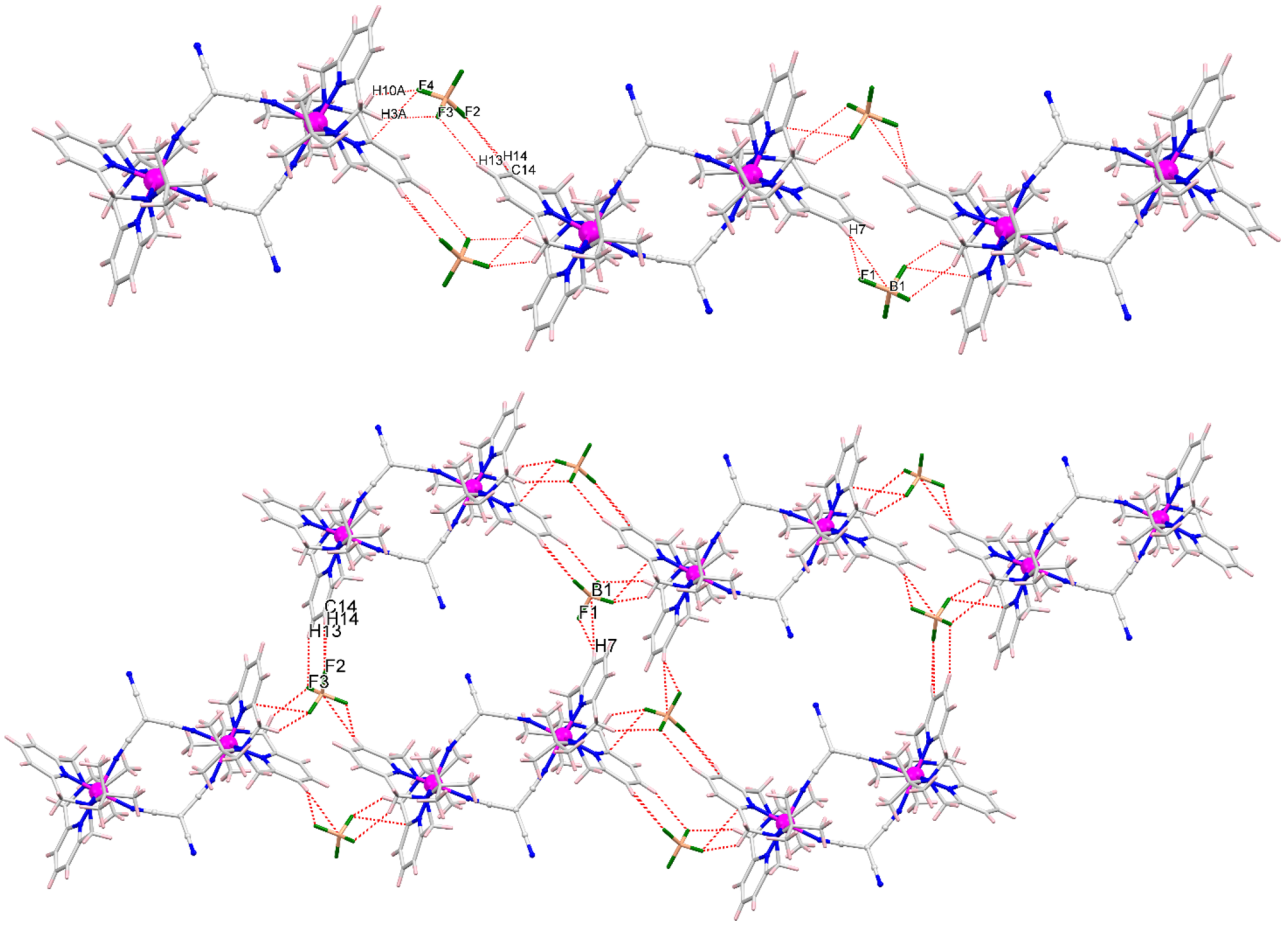

Figure 8. Packing diagrams of **2** at 296 K showing the 1D supramolecular arrangement (top) and the supramolecular double chain (bottom) formed by several C−H···F and C·····F (red dotted lines) interactions (Co, pink; C, gray; N, blue; B, light pink; F, green).

Co−N bond distances play an important role in estimating the spin state over the unaffected axial Co−N_{am} bond distances.

Similarly to complex **1**, the N_{am}−Co−N_{am} angle and N_{Py}−Co−N_{Py} and N_{dca}−Co−N_{dca} angles deviate from 180° to 149.25(9)°, and from 90° to 88.8(1)° and 88.5(1)°, respectively (Table 1 and Table S2). The bridging arrangement of Co−NC−C(CN)−CN−Co adopts a V-shaped conformation with C−C−C angles of 118.5(4) and 116.4(4)° (C(1)−C(25)−C(1) and C(2)−C(27)−C(2), respectively), and the N−C−C angles are almost linear with values of 175.4(4)° and 177.0(4)° (N(5)−C(1)−C(25) and N(6)−C(2)−C(27), respectively). However, Co−N−C angles with values of 157.6(3) and 169.7(3)° deviate from linearity at 296 K. No significant changes have been observed in these values upon cooling to 100 K, while Co···Co distances between two bridged cobalt centers decreases slightly from 7.129 Å (296 K) to 7.082 Å (100 K) upon a decrease in temperature. It is worth mentioning that the significant differences in the bridging V-shaped conformation with C−N−C angle of 125.3(3)° in **1** and C−C−C angles of 118.5(4) and 116.4(4)° in **2** might be the reason for the two distinct molecular structures in **1** and **2**.

The octahedral geometry is significantly altered by the spin state of SCO metal centers. The HS state is more distorted from a perfect octahedron than is the LS state, due to the population of the antibonding orbitals in the HS state. The octahedral distortion parameters[53,56] ($\sum$, θ, and ζ) that describe the extent of octahedral distortion associated with the spin-state changes have been estimated (Table 1). The octahedral distortion parameters ($\sum$, θ, and ζ) at 296 K suggest that the cobalt(II) site in **1** has a more distorted octahedral geometry than in **2** (Table 1). At 100 K, these values for **2** decrease slightly, corresponding to a more regular N_6 coordination environment at low temperature. It is worth mentioning that these values of **1** at 296 K and of **2** at 100 K are very close to those for HS cobalt(II) and LS cobalt(II) complexes, respectively, thereby indicating the HS state in **1** at 296 K and the LS state in **2** at 100 K.[53,56] In addition, the slightly higher values of these parameters for **2** at 296 K indicate the population of a LS/HS mixed state. The distortions of cobalt(II) coordination centers were also determined by CShM using the SHAPE program (Table 1 and Table S3). A shape factor of 0 corresponds to a perfectly octahedral site. The overall outcome of shape factors with low values in the range 2.277−2.428 suggest a deviation from a perfect octahedron in both complexes. The lowering of the shape factors upon a decrease in temperature in complex **2** is in accordance with the results from the octahedral distortion parameters.

In complex **1**, each 1D chain is connected to another 1D chain by several weak C−H···F and C·····F interactions among the coordinated ligand **L**, BF_4^- anions, and methanol molecules, forming a supramolecular double chain (Figure 7 and Table S4). A moderate thermal volume diminution (~3.21%) with a slight contraction along all the three axes and a significant modification of supramolecular interactions have been observed during the occurrence of SCO in **2**. Weak C−H···F and C·····F interactions have been observed, leading to the formation of supramolecular

1D configuration and a double chain in **2** at 296 K (Figure 8 and Table S4). When the temperature is lowered to 100 K, the values of these supramolecular interactions decrease slightly, with the addition of new C−H···F interactions (Figure S7 and Table S4).

Spectroscopic Studies. Electronic spectra of **1** and **2** were recorded in the solid state as well as in solution at room temperature (Figures S8 and S9). The spectrum of **1** in DMF shows two broad bands centered at around 1030 and 550 nm and a shoulder at around 513 nm, which are ascribed to d−d transitions ($^4T_{1g} \rightarrow {}^4T_{2g}(^4F)$, $^4T_{1g} \rightarrow {}^4T_{1g}(^4P)$, and $^4T_{1g} \rightarrow {}^4A_{2g}(^4F)$, respectively) in a HS cobalt(II) ion.[63,64,73] Complex **2** is in a LS/HS mixed state at room temperature (*vide infra*); the spectrum shows two broad bands centered at around 950 and 478 nm which are attributed to d−d transitions. Apart from the d−d transitions, the spectra of both complexes show a ligand to metal charge transfer (LMCT) transition, a metal to ligand charge transfer (MLCT) transition, and an interligand charge transfer (ILCT) transition at around 300−400 and 265 nm, respectively. The solid-state spectra of the complexes display absorption bands similar to those of the solution spectra, indicating that the complexes conserved their individuality in both the solid and solution states.

Magnetic Studies. Magnetic measurements were carried out on polycrystalline samples of **1** and **2** at magnetic fields of 1000 and 10000 Oe respectively, and in the temperature ranges of 2−300 K and 2−400 K for **1** and **2**, respectively in both cooling and heating modes. For complex **1** at 300 K, the measured χT (χ is the magnetic susceptibility equal to M/H per cobalt(II) ion) value is 3.14 $cm^3\ mol^{-1}\ K$ (Figure 9), lying in the

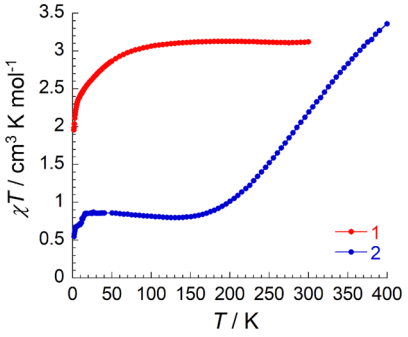

Figure 9. Temperature dependence of χT for **1** and **2** in heating modes.

expected range typically observed for octahedral cobalt(II) ion in the HS state ($\chi T \approx 2.1-3.4\ cm^3\ mol^{-1}\ K$) with a significant orbital contribution.[25,53,63,64,73,74] This value remains nearly constant up to 100 K. Below this temperature, the χT value decreases rapidly to 1.92 $cm^3\ mol^{-1}$ K at 1.85 K (Figure S11, log scale), which is probably due to the combination of magnetic anisotropy, spin−orbit coupling coming from a HS cobalt(II) ion, and also weak antiferromagnetic intra- and intermolecular interactions between the HS cobalt(II) centers.

The field dependence of magnetization was determined for **1** from 0 to 7 T at 1.85, 3, 5, and 8 K (Figure S12). The magnetization value at 1.85 K and 7 T is 2.62 μ_B, which is lower than the expected value for a $S = 3/2$ system. An M vs H/T measurement shows nonsuperposition of the data on a single master curve (Figure S12). The nonsaturation and non-superposition of the magnetization curves suggest the presence of magnetic anisotropy in **1**. It is worth noting that no slow relaxation of magnetization was observed in **1** during ac susceptibility measurements even when a 10000 Oe dc magnetic field was used (Figures S13 and S14).

The experimental magnetic data of **1** have been treated using the spin Hamiltonian, formulated as

$$\hat{H} = D(\hat{S}_z^{\,2} - \hat{S}^2/3) + E(\hat{S}_x^{\,2} - \hat{S}_y^{\,2}) + \mu_B B g \hat{S}_a - zj\langle\hat{S}_a\rangle\hat{S}_a \quad (1)$$

It it comprised of the zero-field splitting terms, a Zeeman term, and the molecular field correction parameter zj to take into account the weak intra-/interchain interactions. An analysis of the experimental data provided the following: $D = -72.3\ cm^{-1}$, $E/D = 0.00$, $g_z = 2.87$, $g_{xy} = 2.21$, and $zj = -0.273\ cm^{-1}$ (Figure S15). Usually, a positive D parameter is expected for pseudo-octahedral cobalt(II) complexes;[75] however, a negative D value has recently been observed in one cobalt(II) complex with azido coligands.[76] Nonetheless, a theoretical CASSCF calculation (*vide infra*) indicates the presence of low-lying excited states originating from the $^4T_{1g}$ state, thus limiting the spin Hamiltonian application, and a more suitable Griffith-Figgis Hamiltonian[77] was then used:

$$\hat{H} = -\alpha\cdot\lambda(\vec{S}\cdot\vec{L}) + \Delta_{ax}(\hat{L}_z^{\,2} - \hat{L}^2/3) + \Delta_{rh}(\hat{L}_x^{\,2} - \hat{L}_y^{\,2}) + \mu_B\vec{B}(g_e\vec{S} - \alpha\vec{L}) - zj\langle\hat{S}_a\rangle\hat{S}_a \quad (2)$$

where Δ_{ax} and Δ_{rh} describe the splitting of the $^4T_{1g}$ state upon lowering the crystal-field symmetry. The best fit was obtained with a fit that resulted in the following parameters: $\Delta_{ax} = -1800\ cm^{-1}$, $\Delta_{rh} = -11.6\ cm^{-1}$, $\alpha = 1.50$, $\lambda = -135\ cm^{-1}$, and $zj = -1.93\ cm^{-1}$ (Figure S16). These parameters are in good agreement with that derived from an analysis of CASSCF/NEVPT2 calculations (*vide infra*).

The χT vs T plot for **2** has been measured up to 400 K, and it exhibits a χT value of 3.36 $cm^3\ mol^{-1}$ K at 400 K, which is lower than the value expected for two HS cobalt(II) ions ($2 \times (2.1-3.4)\ cm^3\ mol^{-1}\ K$).[25,53,63,64,73,74] The χT value decreases smoothly with a decrease in temperature down to 150 K to a value of 0.75 $cm^3\ mol^{-1}$ K and then remains almost constant down to 20 K. This χT value at 20 K is consistent with the expected value for two cobalt(II) ions in a LS state ($S = 2 \times 1/2$, $g = 2.0$; $\chi T = 2 \times 0.35\ cm^3\ mol^{-1}\ K$)).[53,63,64] The changes in χT value indicate an incomplete and gradual HS ($S = 3/2$) to LS ($S = 1/2$) spin-state switching in **2**. With a further decrease in temperature, the χT value decreases to 0.53 $cm^3\ mol^{-1}$ K at 2 K, which is probably due to weak antiferromagnetic intra- and intermolecular interactions between the LS cobalt(II) centers. In cooling mode, the χT vs T curve remains same as that in the heating mode, suggesting a reversible SCO without hysteretic behavior (Figure S17). The χT vs T data were fitted using the ideal solution model (Figure S18), which provides the thermodynamic parameters $\Delta H = 13.3\ (1)$ kJ mol^{-1}, $T_{1/2} = 321(1)$ K, and $\Delta S = \Delta H/T_{1/2} = 40.8\ J\ K^{-1}\ mol^{-1}$ for the spin-crossover phenomenon in **2**. These ΔH and ΔS values are in the ranges of those expected for cobalt(II) SCO systems.[53,63,64] Overall magnetic investigations allow us to conclude that, to the best of our knowledge, complex **2** is the only dinuclear cobalt(II) complex bridged by anionic ligands exhibiting a reversible spin crossover with intramolecular spin−spin interaction properties.

The field-dependent magnetization measurements for **2** were performed from 0 to 5 T at 4 and 8 K (Figure S19). The magnetization value at 4 K and 5 T is 1.28 μ_B, which is lower than the expected value for two $S = 1/2$ systems. The lower value might be due to the antiferromagnetic interaction at low

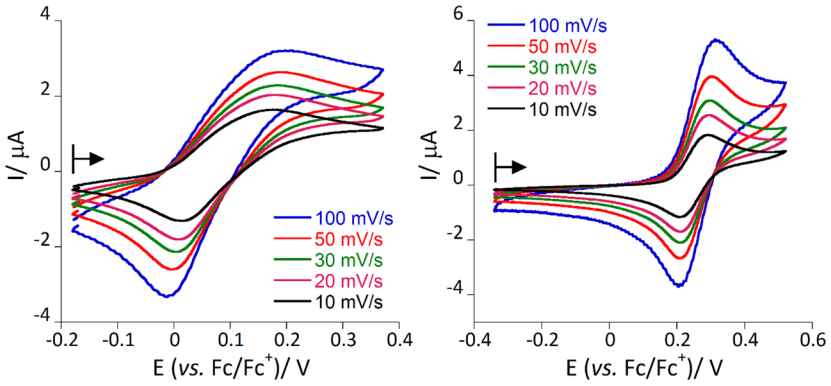

Figure 10. Cyclic voltammograms for the oxidation of **1** (left) and **2** (right) in 0.2 M (^{n}Bu$_4$N)PF$_6$/DMF at various scan rates. Arrows indicate the open circuit potential along with the direction of the potential sweep.

temperature. In addition, M vs H/T measurements display nonsuperposition of the data on a single master curve (Figure S19), confirming low-lying excited states or magnetic anisotropy of the LS cobalt(II) in **2**. No hysteresis was observed in M vs H at 2 K from −70000 to +70000 Oe with a sweep rate of 100−600 Oe/min.

Electrochemical Studies. Redox stimulus prompts the spin-state switching between the paramagnetic HS cobalt(II) (S = 3/2) to diamagnetic LS cobalt(III) (S = 0), offering an alternative way to switch the magnetic properties.[60,63,64] Accordingly, the electrochemical properties of complexes **1** and **2** were investigated by cyclic voltammetry, square wave voltammetry, and differential pulse voltammetry in DMF using 0.2 M (^{n}Bu$_4$N)PF$_6$ as an electrolyte (Figure 10 and Figures S20−S27). Voltammograms of complex **1** reveal two quasi-reversible peaks with $E_{1/2}$ values of 0.1 V (E_{pc} = 0.19 V, E_{pa} = −0.01 V, and ΔE = 0.20 V) and −1.67 V vs Fc/Fc$^+$ (E_{pc} = −1.60 V, E_{pa} = −1.74 V, and ΔE = 0.14 V). The former $E_{1/2}$ value suggests the oxidation of the HS cobalt(II) center to LS cobalt(III), while the latter $E_{1/2}$ value indicates the reduction of the macrocyclic ligand **L**, resulting in a Co(II)-stabilized ligand anion radical.[63,64] Voltammograms of complex **2** exhibit a quasi-reversible oxidation of the cobalt(II) centers with an $E_{1/2}$ value of 0.26 V (E_{pc} = 0.31 V, E_{pa} = 0.21 V, and ΔE = 0.10 V), while several irreversible reductions have been observed for complex **2**.

Theoretical Analyses. Detailed theoretical investigations of the electronic structure of **1** and **2** were performed with ORCA 4.2 software.[78] The magnetic interactions between cobalt(II) centers were assessed by DFT methods with the B3LYP functional by employing the broken-symmetry approach to dinuclear molecular fragments on the basis of experimental X-ray data (Figure 11). The calculations suggest that the spin densities of **1** and **2** are mainly located on metal centers with weak magnetic interaction through bridging pseudohalides with a value of J = +0.26 cm^{-1} for **1** and J = −1.32 cm^{-1} for **2**.

Next, multireference calculations, CASSCF with two types of dynamic correlation treatments, NEVPT2 and DCD-CAS(2), were carried out for the mononuclear fragment of **1**. The calculations revealed D = −100 cm^{-1} and E/D = 0.262 with g values of g_x = 2.270, g_y = 1.790, and g_z = 3.088 for CASSCF/NEVPT2 and D = −95.1 cm^{-1} and E/D = 0.269 for CASSCF/DCD-CAS(2). The D tensor axes are depicted in Figure 12, in which the calculated three-dimensional plot of the molar magnetization is also overlaid over the molecular structure, showing the axial type of magnetic anisotropy in **1**.

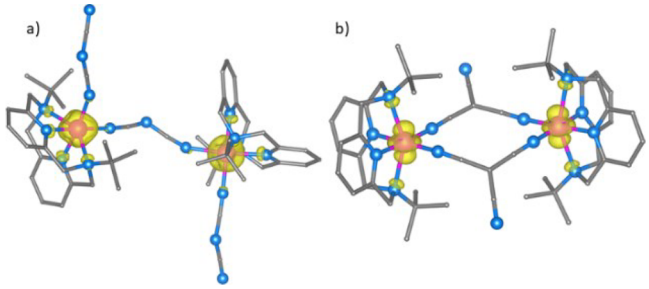

Figure 11. Calculated spin isodensity surfaces using B3LYP for $[Co_2(\mathbf{L})_2(N(CN)_2)_3]^+$ of **1** (a) and $[Co_2(\mathbf{L})_2(C(CN)_3)_2]^{2+}$ of **2** (b). Positive spin densities are represented by yellow surfaces with cutoff values of 0.01 e bohr^{-3}.

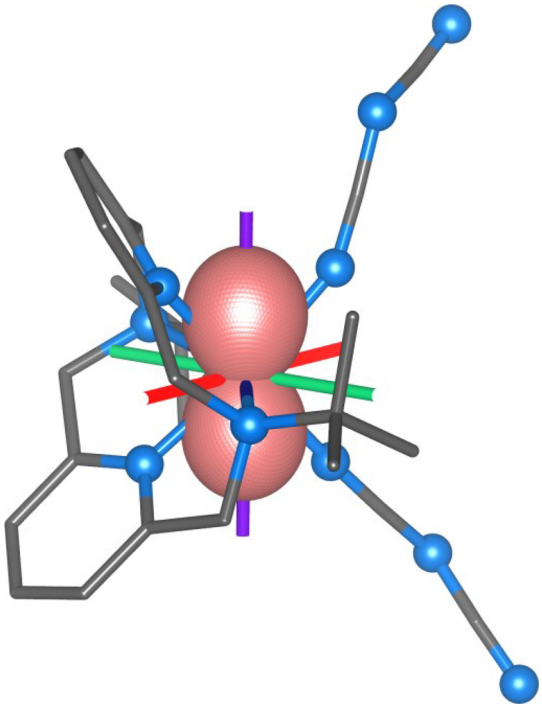

Figure 12. Molecular fragment $[Co(\mathbf{L})(N(CN)_2)_2]$ of **1** overlaid with the principal axis of the D tensor (x, y, and z axes are shown as red, green, and violet lines, respectively) and the three-dimensional molar magnetization (pink surface) calculated for T = 2 K and B = 0.3 T resulting from CASSCF/NEVPT calculations.

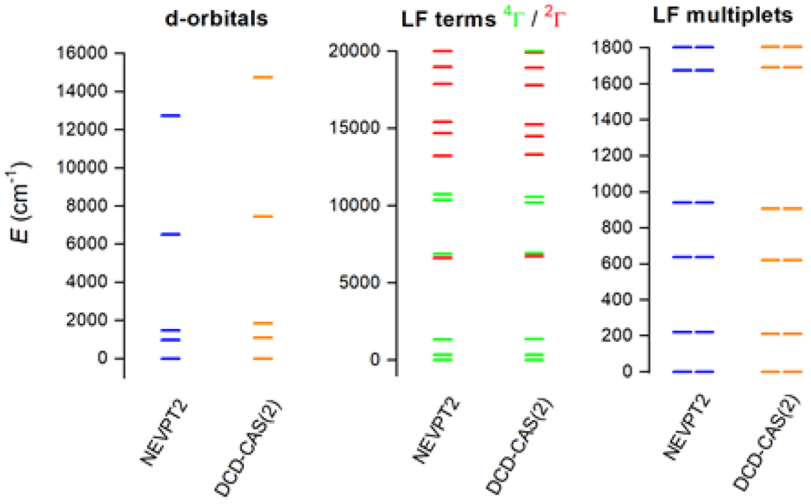

Figure 13. Pictorial presentation of the CASSCF/NEVPT and CASSCF/DCD-CAS(2) with CAS(7,5) calculations for the molecular fragment $[Co(\mathbf{L})(N(CN)_2)_2]$ of **1**: (left) plot of the d orbital splitting using ab initio ligand field theory (AILFT) calculations; (middle) low-lying ligand-field terms with different multiplicities; (right) ligand-field multiplets displaying zero-field splitting.

However, for complex **1** the calculated *g* tensor and *D* tensor parameters might not be perfectly appropriate because of the presence of low-lying excited states (Figure 13), which limits the application of the spin Hamiltonian method.

Therefore, the energies of the six lowest Kramers doublets were analyzed using the Griffith−Figgis[79] model, providing us with the parameters $\alpha\cdot\lambda = -261$ cm^{-1}, $\Delta_{ax} = -1121$ cm^{-1}, and $\Delta_{rh} = -186$ cm^{-1} and $\alpha\cdot\lambda = -251$ cm^{-1}, $\Delta_{ax} = -1166$ cm^{-1}, and $\Delta_{rh} = -184$ cm^{-1} with CASSCF/NEVPT2 and CASSCF/DCD-CAS(2), respectively.

CONCLUSION

In conclusion, herein we presented two new cobalt(II) complexes based on a neutral tetradentate macrocyclic ligand (**L**) where two different nonlinear pseudohalides, i.e. $[N(CN)_2]^-$ and $[C(CN)_3]^-$, have been used as bridging ligands for selective tuning of the ligand field strength around the cobalt(II) centers. The use of $[N(CN)_2]^-$ led to a 1D coordination polymer through a $\mu_{1,5}$-bidentate bridging mode of $[N(CN)_2]^-$. However a discrete dinuclear cobalt(II) complex was formed by the use of the pseudohalide $[C(CN)_3]^-$ as a bridging ligand connecting two cobalt(II) centers via a $\mu_{1,5}$-bidentate bridging mode. The cobalt(II) centers in coordination polymer **1** are in a HS state over the entire temperature range, exhibiting a weak magnetic interaction between the cobalt(II) centers with a large magnetic anisotropy. However, the dinuclear discrete complex shows a reversible and gradual HS to LS spin crossover, which is in accordance with the order of the ligand field strength of the bridging ligands: i.e., $[N(CN)_2]^- < [C(CN)_3]^-$. In addition, the dinuclear complex shows a weak antiferromagnetic interaction between the LS cobalt(II) centers. Both complexes exhibit redox-stimuli-based reversible paramagnetic HS cobalt(II) to diamagnetic LS cobalt(III) conversion, offering an additional way to switch the magnetic properties. This detailed study allows us to conclude that, to the best of our knowledge, the dinuclear complex represents the only known complex involving bridging anionic ligands displaying both spin crossover and spin exchange behaviors in a cobalt system. Theoretical calculations are also consistent with the results stated above.

EXPERIMENTAL SECTION

Detailed experimental procedures, including materials and physical measurements, magnetic measurements, X-ray crystallography, and theoretical calculations, are described in the Supporting Information.

Synthesis of Complexes. *Synthesis of {[Co(L)($\mu_{1,5}$-dca)]BF_4·MeOH}$_n$ (**1**).* Under an argon atmosphere, a mixture of $Co(BF_4)_2\cdot 6H_2O$ (36 mg, 0.1 mmol) and ligand **L** (38 mg, 0.1 mmol) in a mixture of methanol and dichloromethane (ratio 1:1) (10 mL) was stirred for 2 h. Solid $Na[N(CN)_2]$ (9 mg, 0.1 mmol) was added to the solution (Scheme 1). After it was stirred for 2 h, the resulting reaction mixture was filtered. Slow evaporation of the filtrate gave pink crystals of **1** (Figure 1) in 87% yield. Anal. Calcd for $C_{25}H_{36}CoN_7BF_4O$ (MW 596.35 g mol^{-1}): C, 50.35; H, 6.09; N, 16.44. Found: C, 50.07; H, 6.25; N, 16.62. ATR-IR (only intense bands): ν (cm^{-1}) 3553, 2975, 2312, 2244, 2217, 2910, 2171, 1603, 1468, 1468, 1384, 1193, 1165, 1061, 1028, 939, 916, 851, 789, 712, 646, 507. UV−vis−NIR (solid state, KBr): λ_{max} (nm) 267, 350, 435, 514, 555, 1012.

*Synthesis of [Co_2(L)$_2$($\mu_{1,5}$-tcm)$_2$](BF_4)$_2$ (**2**).* Under an argon atmosphere, a mixture of $Co(BF_4)_2\cdot 6H_2O$ (36 mg, 0.1 mmol) and ligand **L** (38 mg, 0.1 mmol) in methanol and dichloromethane (ratio 1:1) (10 mL) was stirred for 2 h. Solid $Na[C(CN)_3]$ (11.5 mg, 0.1 mmol) was added to the solution (Scheme S1). After it was stirred for an additional 2 h, the resulting reaction mixture was filtered. Slow evaporation of the filtrate gave orange crystals of **2** (Figure S1) in 82% yield. Anal. Calcd for $C_{52}H_{64}B_2Co_2F_8N_{14}$ (M.W 1176.65 g mol^{-1}): C, 53.08; H, 5.48; N, 16.67. Found: C, 52.89; H, 5.23; N, 16.46. ATR-IR (only intense bands): ν (cm^{-1}): 2977, 2224, 2190, 2171, 1606, 1469, 1442, 1377, 1253, 1187, 1026, 916, 849, 791, 560, 520, 481. UV−vis−NIR (solid state, KBr): λ_{max} (nm) 265, 345, 409, 482, 950.

ASSOCIATED CONTENT

Supporting Information

The Supporting Information is available free of charge at https://pubs.acs.org/doi/10.1021/acs.inorgchem.0c02887.

Experimental, spectral, and crystallographic data (PDF)

Accession Codes

CCDC 2005150−2005152 contain the supplementary crystallographic data for this paper. These data can be obtained free of charge via www.ccdc.cam.ac.uk/data_request/cif, or by emailing data_request@ccdc.cam.ac.uk, or by contacting The Cambridge Crystallographic Data Centre, 12 Union Road, Cambridge CB2 1EZ, UK; fax: +44 1223 336033.

AUTHOR INFORMATION

Corresponding Author

Abhishake Mondal − *Solid State and Structural Chemistry Unit, Indian Institute of Science, Bangalore 560012, India;* orcid.org/0000-0002-5061-2326; Email: mondal@iisc.ac.in

Authors

Subrata Ghosh − *Solid State and Structural Chemistry Unit, Indian Institute of Science, Bangalore 560012, India;* orcid.org/0000-0003-4539-4413

Sujit Kamilya − *Solid State and Structural Chemistry Unit, Indian Institute of Science, Bangalore 560012, India;* orcid.org/0000-0003-4881-0638

Mathieu Rouzières − *Univ. Bordeaux, CNRS, Centre de Recherche Paul Pascal, CRPP, UMR 5031, 33600 Pessac, France*

Radovan Herchel − *Department of Inorganic Chemistry, Faculty of Science, Palacký University, CZ-771 46 Olomouc, Czech Republic;* orcid.org/0000-0001-8262-4666

Sakshi Mehta − *Solid State and Structural Chemistry Unit, Indian Institute of Science, Bangalore 560012, India*

Complete contact information is available at: https://pubs.acs.org/10.1021/acs.inorgchem.0c02887

Notes

The authors declare no competing financial interest.

ACKNOWLEDGMENTS

This research work was supported by the Indian Institute of Science (IISc), Bangalore, India, and the Science & Engineering Research Board (SERB) (Project No. SRG/2019/000317). We are thankful to the IISc for funding a Start-up Research Grant. S.G. and S.M. thank the IISc and S.K. thanks the Council of Scientific & Industrial Research (CSIR), Government of India, for their fellowships.

REFERENCES

(1) Coronado, E. Molecular magnetism: from chemical design to spin control in molecules, materials and devices. *Nat. Rev. Mater.* **2020**, *5*, 87−104.

(2) Ferrando-Soria, J.; Vallejo, J.; Castellano, M.; Martínez-Lillo, J.; Pardo, E.; Cano, J.; Castro, I.; Lloret, F.; Ruiz-García, R.; Julve, M. Molecular magnetism, quo vadis? A historical perspective from a coordination chemist viewpoint☆. *Coord. Chem. Rev.* **2017**, *339*, 17−103.

(3) Yao, Z.-S.; Tang, Z.; Tao, J. Bistable molecular materials with dynamic structures. *Chem. Commun.* **2020**, *56*, 2071−2086.

(4) Koebke, A.; Gutzeit, F.; Roehricht, F.; Schlimm, A.; Grunwald, J.; Tuczek, F.; Studniarek, M.; Longo, D.; Choueikani, F.; Otero, E.; Ohresser, P.; Rohlf, S.; Johannsen, S.; Diekmann, F.; Rossnagel, K.; Weismann, A.; Jasper-Toennies, T.; Naether, C.; Herges, R.; Berndt, R.; Gruber, M. Reversible coordination-induced spin-state switching in complexes on metal surfaces. *Nat. Nanotechnol.* **2020**, *15*, 18−21.

(5) Bigdeli, F.; Lollar, C. T.; Morsali, A.; Zhou, H.-C. Switching in Metal-Organic Frameworks. *Angew. Chem., Int. Ed.* **2020**, *59*, 4652−4669.

(6) Szuromi, P. Coherent surface spin manipulation. *Science* **2019**, *366*, 440−442.

(7) Meng, Y.-S.; Liu, T. Manipulating Spin Transition To Achieve Switchable Multifunctions. *Acc. Chem. Res.* **2019**, *52*, 1369−1379.

(8) Molnár, G.; Rat, S.; Salmon, L.; Nicolazzi, W.; Bousseksou, A. Spin Crossover Nanomaterials: From Fundamental Concepts to Devices. *Adv. Mater.* **2018**, *30*, 1703862−1703884.

(9) Senthil Kumar, K.; Ruben, M. Emerging trends in spin crossover (SCO) based functional materials and devices. *Coord. Chem. Rev.* **2017**, *346*, 176−205.

(10) Khusniyarov, M. M. How to Switch Spin-Crossover Metal Complexes at Constant Room Temperature. *Chem. - Eur. J.* **2016**, *22*, 15178−15191.

(11) Aromi, G.; Real, J. A. Special Issue "Spin Crossover (SCO) Research. *Magnetochemistry* **2016**, *2*, 28−30.

(12) Marin, R.; Brunet, G.; Murugesu, M. Shining new light on multifunctional lanthanide single-molecule magnets. *Angew. Chem., Int. Ed.* **2020**, DOI: 10.1002/anie.201910299.

(13) Sørensen, M. A.; Hansen, U. B.; Perfetti, M.; Pedersen, K. S.; Bartolomé, E.; Simeoni, G. G.; Mutka, H.; Rols, S.; Jeong, M.; Zivkovic, I.; Retuerto, M.; Arauzo, A.; Bartolomé, J.; Piligkos, S.; Weihe, H.; Doerrer, L. H.; van Slageren, J.; Rønnow, H. M.; Lefmann, K.; Bendix, J. Chemical tunnel-splitting-engineering in a dysprosium-based molecular nanomagnet. *Nat. Commun.* **2018**, *9*, 1292−1300.

(14) Feng, M.; Tong, M.-L. Single Ion Magnets from 3d to 5f: Developments and Strategies. *Chem. - Eur. J.* **2018**, *24*, 7574−7594.

(15) Goodwin, C. A. P.; Ortu, F.; Reta, D.; Chilton, N. F.; Mills, D. P. Molecular magnetic hysteresis at 60 K in dysprosocenium. *Nature* **2017**, *548*, 439−442.

(16) Woodruff, D. N.; Winpenny, R. E. P.; Layfield, R. A. Lanthanide Single-Molecule Magnets. *Chem. Rev.* **2013**, *113*, 5110−5148.

(17) Sessoli, R.; Gatteschi, D.; Caneschi, A.; Novak, M. A. Magnetic bistability in a metal-ion cluster. *Nature* **1993**, *365*, 141−143.

(18) Houard, F.; Evrard, Q.; Calvez, G.; Suffren, Y.; Daiguebonne, C.; Guillou, O.; Gendron, F.; Le Guennic, B.; Guizouarn, T.; Dorcet, V.; Mannini, M.; Bernot, K. Chiral Supramolecular Nanotubes of Single-Chain Magnets. *Angew. Chem., Int. Ed.* **2020**, *59*, 780−784.

(19) Coulon, C.; Miyasaka, H.; Clérac, R. In *Single-Molecule Magnets and Related Phenomena*; Winpenny, R., Ed.; Springer Berlin Heidelberg: Berlin, Heidelberg, 2006; pp 163−206.

(20) Lutz, P.; Aguilà, D.; Mondal, A.; Pinkowicz, D.; Marx, R.; Neugebauer, P.; Fåk, B.; Ollivier, J.; Clérac, R.; van Slageren, J. Elementary excitations in single-chain magnets. *Phys. Rev. B: Condens. Matter Mater. Phys.* **2017**, *96*, 094415−094420.

(21) Mathonière, C. Metal-to-Metal Electron Transfer: A Powerful Tool for the Design of Switchable Coordination Compounds. *Eur. J. Inorg. Chem.* **2018**, *2018*, 248−258.

(22) Sato, O. Dynamic molecular crystals with switchable physical properties. *Nat. Chem.* **2016**, *8*, 644−656.

(23) Aguilà, D.; Prado, Y.; Koumousi, E. S.; Mathonière, C.; Clérac, R. Switchable Fe/Co Prussian blue networks and molecular analogues. *Chem. Soc. Rev.* **2016**, *45*, 203−224.

(24) Sato, O.; Iyoda, T.; Fujishima, A.; Hashimoto, K. Photoinduced Magnetization of a Cobalt-Iron Cyanide. *Science* **1996**, *272*, 704−705.

(25) Mondal, A.; Li, Y.; Seuleiman, M.; Julve, M.; Toupet, L.; Buron-Le Cointe, M.; Lescouezec, R. On/Off Photoswitching in a Cyanide-Bridged $\{Fe_2Co_2\}$ Magnetic Molecular Square. *J. Am. Chem. Soc.* **2013**, *135*, 1653−1656.

(26) Kamilya, S.; Ghosh, S.; Li, Y.; Dechambenoit, P.; Rouzieres, M.; Lescouezec, R.; Mehta, S.; Mondal, A. Two-Step Thermoinduced Metal-to-Metal Electron Transfer and ON/OFF Photoswitching in a Molecular $[Fe_2Co_2]$ Square Complex. *Inorg. Chem.* **2020**, *59*, 11879−11888.

(27) Wang, Y.; Wang, S.; Wang, X.; Zhang, W.; Zheng, W.; Zhang, Y.-M.; Zhang, S. X.-A. A multicolour bistable electronic shelf label based on intramolecular proton-coupled electron transfer. *Nat. Mater.* **2019**, *18*, 1335−1342.

(28) Dragulescu-Andrasi, A.; Filatov, A. S.; Oakley, R. T.; Li, X.; Lekin, K.; Huq, A.; Pak, C.; Greer, S. M.; McKay, J.; Jo, M.; Lengyel, J.; Hung, I.; Maradzike, E.; DePrince, A. E.; Stoian, S. A.; Hill, S.; Hu, Y.-Y.; Shatruk, M. Radical Dimerization in a Plastic Organic Crystal Leads to Structural and Magnetic Bistability with Wide Thermal Hysteresis. *J. Am. Chem. Soc.* **2019**, *141*, 17989−17994.

(29) Manrique-Juarez, M. D.; Mathieu, F.; Shalabaeva, V.; Cacheux, J.; Rat, S.; Nicu, L.; Leichle, T.; Salmon, L.; Molnar, G.; Bousseksou, A. A

Bistable Microelectromechanical System Actuated by Spin-Crossover Molecules. *Angew. Chem., Int. Ed.* **2017**, *56*, 8074−8078.
(30) Estrader, M.; Salinas Uber, J.; Barrios, L. A.; Garcia, J.; Lloyd-Williams, P.; Roubeau, O.; Teat, S. J.; Aromi, G. A Magneto-optical Molecular Device: Interplay of Spin Crossover, Luminescence, Photomagnetism, and Photochromism. *Angew. Chem., Int. Ed.* **2017**, *56*, 15622−15627.
(31) Kucheriv, O. I.; Oliynyk, V. V.; Zagorodnii, V. V.; Launets, V. L.; Gural'skiy, I. y. A. Spin-Crossover Materials towards Microwave Radiation Switches. *Sci. Rep.* **2016**, *6*, 38334−38340.
(32) Kahn, O.; Martinez, C. J. Spin-Transition Polymers: From Molecular Materials Toward Memory Devices. *Science* **1998**, *279*, 44−48.
(33) Kahn, O.; Kröber, J.; Jay, C. Spin Transition Molecular Materials for displays and data recording. *Adv. Mater.* **1992**, *4*, 718−728.
(34) Kitazawa, T. Synthesis and Applications of New Spin Crossover Compounds. *Crystals* **2019**, *9*, 382−385.
(35) Halcrow, M. A. *Spin-crossover materials properties and applications*; Wiley: Chichester, U.K., 2013.
(36) Gütlich, P.; Gaspar, A. B.; Garcia, Y. Spin state switching in iron coordination compounds. *Beilstein J. Org. Chem.* **2013**, *9*, 342−391.
(37) Gütlich, P.; Goodwin, H. A. *Spin Crossover in Transition Metal Compounds III*; Springer: New York, 2006.
(38) Gütlich, P.; Hauser, A.; Spiering, H. Thermal and Optical Switching of Iron(II) Complexes. *Angew. Chem., Int. Ed. Engl.* **1994**, *33*, 2024−2054.
(39) Scott, H. S.; Staniland, R. W.; Kruger, P. E. Spin crossover in homoleptic Fe(II) imidazolylimine complexes. *Coord. Chem. Rev.* **2018**, *362*, 24−43.
(40) Hogue, R. W.; Singh, S.; Brooker, S. Spin crossover in discrete polynuclear iron(II) complexes. *Chem. Soc. Rev.* **2018**, *47*, 7303−7338.
(41) Galán Mascarós, J. R.; Aromí, G.; Darawsheh, M. Polynuclear Fe(II) complexes: Di/trinuclear molecules and coordination networks. *C. R. Chim.* **2018**, *21*, 1209−1229.
(42) Ni, Z.-P.; Liu, J.-L.; Hoque, M. N.; Liu, W.; Li, J.-Y.; Chen, Y.-C.; Tong, M.-L. Recent advances in guest effects on spin-crossover behavior in Hofmann-type metal-organic frameworks. *Coord. Chem. Rev.* **2017**, *335*, 28−43.
(43) Feltham, H. L. C.; Barltrop, A. S.; Brooker, S. Spin crossover in iron(II) complexes of 3,4,5-tri-substituted-1,2,4-triazole (Rdpt), 3,5-di-substituted-1,2,4-triazolate (dpt−), and related ligands. *Coord. Chem. Rev.* **2017**, *344*, 26−53.
(44) Harding, D. J.; Harding, P.; Phonsri, W. Spin crossover in iron(III) complexes. *Coord. Chem. Rev.* **2016**, *313*, 38−61.
(45) Kershaw Cook, L. J.; Mohammed, R.; Sherborne, G.; Roberts, T. D.; Alvarez, S.; Halcrow, M. A. Spin state behavior of iron(II)/dipyrazolylpyridine complexes. New insights from crystallographic and solution measurements. *Coord. Chem. Rev.* **2015**, *289*−*290*, 2−12.
(46) Mondal, A.; Li, Y.; Chamoreau, L.-M.; Seuleiman, M.; Rechignat, L.; Bousseksou, A.; Boillot, M.-L.; Lescouëzec, R. Photo- and thermo-induced spin crossover in a cyanide-bridged $\{Mo^{V}_{2}Fe^{II}_{2}\}$ rhombus molecule. *Chem. Commun.* **2014**, *50*, 2893−2895.
(47) Mondal, A.; Li, Y.; Herson, P.; Seuleiman, M.; Boillot, M.-L.; Rivière, E.; Julve, M.; Rechignat, L.; Bousseksou, A.; Lescouëzec, R. Photomagnetic effect in a cyanide-bridged mixed-valence $\{Fe^{II}_{2}Fe^{III}_{2}\}$ molecular square. *Chem. Commun.* **2012**, *48*, 5653−5655.
(48) Ghosh, S.; Kamilya, S.; Pramanik, T.; Rouzieres, M.; Herchel, R.; Mehta, S.; Mondal, A. ON/OFF Photoswitching and Thermoinduced Spin Crossover with Cooperative Luminescence in a 2D Iron(II) Coordination Polymer. *Inorg. Chem.* **2020**, *59*, 13009−13013.
(49) Drath, O.; Boskovic, C. Switchable cobalt coordination polymers: Spin crossover and valence tautomerism. *Coord. Chem. Rev.* **2018**, *375*, 256−266.
(50) Brooker, S. Spin crossover with thermal hysteresis: practicalities and lessons learnt. *Chem. Soc. Rev.* **2015**, *44*, 2880−2892.
(51) Hayami, S.; Komatsu, Y.; Shimizu, T.; Kamihata, H.; Lee, Y. H. Spin-crossover in cobalt(II) compounds containing terpyridine and its derivatives. *Coord. Chem. Rev.* **2011**, *255*, 1981−1990.
(52) Krivokapic, I.; Zerara, M.; Daku, M. L.; Vargas, A.; Enachescu, C.; Ambrus, C.; Tregenna-Piggott, P.; Amstutz, N.; Krausz, E.; Hauser, A. Spin-crossover in cobalt(II) imine complexes. *Coord. Chem. Rev.* **2007**, *251*, 364−378.
(53) Olguín, J. Unusual metal centres/coordination spheres in spin crossover compounds. *Coord. Chem. Rev.* **2020**, *407*, 213148−213177.
(54) Halcrow, M. A. Jahn−Teller distortions in transition metal compounds, and their importance in functional molecular and inorganic materials. *Chem. Soc. Rev.* **2013**, *42*, 1784−1795.
(55) Shao, D.; Shi, L.; Shen, F.-X.; Wei, X.-Q.; Sato, O.; Wang, X.-Y. Reversible On−Off Switching of the Hysteretic Spin Crossover in a Cobalt(II) Complex via Crystal to Crystal Transformation. *Inorg. Chem.* **2019**, *58*, 11589−11598.
(56) McPherson, J. N.; Hogue, R. W.; Akogun, F. S.; Bondì, L.; Luis, E. T.; Price, J. R.; Garden, A. L.; Brooker, S.; Colbran, S. B. Predictable Substituent Control of $Co^{III/II}$ Redox Potential and Spin Crossover in Bis(dipyridylpyrrolide)cobalt Complexes. *Inorg. Chem.* **2019**, *58*, 2218−2228.
(57) Shao, D.; Shi, L.; Yin, L.; Wang, B.-L.; Wang, Z.-X.; Zhang, Y.-Q.; Wang, X.-Y. Reversible on−off switching of both spin crossover and single-molecule magnet behaviours via a crystal-to-crystal transformation. *Chem. Sci.* **2018**, *9*, 7986−7991.
(58) Jeon, I.-R.; Calancea, S.; Panja, A.; Piñero Cruz, D. M.; Koumousi, E. S.; Dechambenoit, P.; Coulon, C.; Wattiaux, A.; Rosa, P.; Mathonière, C.; Clérac, R. Spin crossover or intra-molecular electron transfer in a cyanido-bridged Fe/Co dinuclear dumbbell: a matter of state. *Chem. Sci.* **2013**, *4*, 2463−2470.
(59) Graf, M.; Wolmershäuser, G.; Kelm, H.; Demeschko, S.; Meyer, F.; Krüger, H.-J. Temperature-Induced Spin-Transition in a Low-Spin Cobalt(II) Semiquinonate Complex. *Angew. Chem., Int. Ed.* **2010**, *49*, 950−953.
(60) Cowan, M. G.; Olguín, J.; Narayanaswamy, S.; Tallon, J. L.; Brooker, S. Reversible Switching of a Cobalt Complex by Thermal, Pressure, and Electrochemical Stimuli: Abrupt, Complete, Hysteretic Spin Crossover. *J. Am. Chem. Soc.* **2012**, *134*, 2892−2894.
(61) Roy, S.; Choubey, S.; Bhar, K.; Sikdar, N.; Costa, J. S.; Mitra, P.; Ghosh, B. K. Counter anion dependent gradual spin transition in a 1D cobalt(ii) coordination polymer. *Dalton Trans.* **2015**, *44*, 7774−7776.
(62) Bhar, K.; Khan, S.; Costa, J. S.; Ribas, J.; Roubeau, O.; Mitra, P.; Ghosh, B. K. Crystallographic Evidence for Reversible Symmetry Breaking in a Spin-Crossover d^7 Cobalt(II) Coordination Polymer. *Angew. Chem., Int. Ed.* **2012**, *51*, 2142−2145.
(63) Ghosh, S.; Selvamani, S.; Mehta, S.; Mondal, A. Reversible thermo-induced spin crossover in a mononuclear cis-dicyanamido-cobalt(ii) complex containing a macrocyclic tetradentate ligand. *Dalton Trans.* **2020**, *49*, 9208−9212.
(64) Ghosh, S.; Selvamani, S.; Kamilya, S.; Mehta, S.; Mondal, A. Tuning of Spin Crossover Properties in a Series of Mononuclear Cobalt(II) Complexes Based on Macrocyclic Tetradentate Ligand and Pseudohalide Coligands. *Dalton Trans.* **2020**, DOI: 10.1039/D0DT02546A.
(65) Milin, E.; Belaid, S.; Patinec, V.; Triki, S.; Chastanet, G.; Marchivie, M. Dinuclear Spin-Crossover Complexes Based on Tetradentate and Bridging Cyanocarbanion Ligands. *Inorg. Chem.* **2016**, *55*, 9038−9046.
(66) Batten, S. R.; Bjernemose, J.; Jensen, P.; Leita, B. A.; Murray, K. S.; Moubaraki, B.; Smith, J. P.; Toftlund, H. Designing dinuclear iron(ii) spin crossover complexes. Structure and magnetism of dinitrile-, dicyanamido-, tricyanomethanide-, bipyrimidine- and tetrazine-bridged compounds. *Dalton Trans.* **2004**, 3370−3375.
(67) Batten, S. R.; Murray, K. S. Structure and magnetism of coordination polymers containing dicyanamide and tricyanomethanide. *Coord. Chem. Rev.* **2003**, *246*, 103−130.
(68) Brooker, S.; Plieger, P. G.; Moubaraki, B.; Murray, K. S. $[Co^{II}_{2}L(NCS)_{2}(SCN)_{2}]$: The First Cobalt Complex to Exhibit Both Exchange Coupling and Spin Crossover Effects. *Angew. Chem., Int. Ed.* **1999**, *38*, 408−410.
(69) Ma, X.; Suturina, E. A.; De, S.; Négrier, P.; Rouzières, M.; Clérac, R.; Dechambenoit, P. A Redox-Active Bridging Ligand to Promote Spin

Delocalization, High-Spin Complexes, and Magnetic Multi-Switchability. *Angew. Chem., Int. Ed.* **2018**, *57*, 7841−7845.
(70) Kohout, J.; Jäger, L.; Hvastijová, M.; Kožíšek, J. Tricyanomethanide and Dicyanamide Complexes of Cu(II), Ni(II), Co(II), Their Structures and Properties. *J. Coord. Chem.* **2000**, *51*, 169−218.
(71) Casanova, D.; Llunell, M.; Alemany, P.; Alvarez, S. *Chem. - Eur. J.* **2005**, *11*, 1479−1494.
(72) Meneghetti, S. P.; Lutz, P. J.; Fischer, J.; Kress, J. Synthesis and X-ray structure of a monoprotonated salt and of three transition-metal complexes of N,N′-ditertiobutyl-2,11-diaza[3.3](2,6)pyridinophane. *Polyhedron* **2001**, *20*, 2705−2710.
(73) Ghosh, S.; Kamilya, S.; Das, M.; Mehta, S.; Boulon, M. E.; Nemec, I.; Rouzieres, M.; Herchel, R.; Mondal, A. Effect of Coordination Geometry on Magnetic Properties in a Series of Cobalt(II) Complexes and Structural Transformation in Mother Liquor. *Inorg. Chem.* **2020**, *59*, 7067−7081.
(74) Mondal, A.; Chamoreau, L.-M.; Li, Y.; Journaux, Y.; Seuleiman, M.; Lescouëzec, R. W-Co Discrete Complex Exhibiting Photo- and Thermo-Induced Magnetisation. *Chem. - Eur. J.* **2013**, *19*, 7682−7685.
(75) Titiš, J.; Boča, R. Magnetostructural D Correlations in Hexacoordinated Cobalt(II) Complexes. *Inorg. Chem.* **2011**, *50*, 11838−11845.
(76) Váhovská, L.; Bukrynov, O.; Potočňák, I.; Čižmár, E.; Kliuikov, A.; Vitushkina, S.; Dušek, M.; Herchel, R. New Cobalt(II) Field-Induced Single-Molecule Magnet and the First Example of a Cobalt(III) Complex with Tridentate Binding of a Deprotonated 4-Amino-3,5-bis(pyridin-2-yl)-1,2,4-Triazole Ligand. *Eur. J. Inorg. Chem.* **2019**, *2019*, 250−261.
(77) Boca, R. *A handbook of magnetochemical formulae*; Elsevier: Oxford, 2012.
(78) Neese, F. Software update: the ORCA program system, version 4.0. *Wiley Interdiscip. Rev.: Comput. Mol. Sci.* **2018**, *8*, e1327.
(79) Nemec, I.; Herchel, R.; Trávníček, Z. Two polymorphic Co(ii) field-induced single-ion magnets with enormous angular distortion from the ideal octahedron. *Dalton Trans.* **2018**, *47*, 1614−1623.